

Anodization of nanoimprinted titanium: a comparison with formation of porous alumina

Jinsub Choi^{a,*}, Ralf B. Wehrspohn^{a,b}, Jaeyoung Lee^{c,2}, Ulrich Gösele^a

^a Max Planck Institute of Microstructure Physics, Weinberg 2, 06120 Halle, Germany

^b Nanophotonic Materials Group, Department of Physics, University of Paderborn, Warburger Strasse 100, 33098 Paderborn, Germany

^c Water Protection Research Team, Research Institute of Industrial Science and Technology, Pohang City 790-330, South Korea

Received 9 December 2003; received in revised form 4 February 2004; accepted 14 February 2004

Abstract

Electrochemically prepared ordered porous alumina has become one of the most important nanotemplate materials to date. Naturally the questions arises whether other valve metals such as Ti, Ta, Nb, V, Hf or W can also be used for fabricating ordered pore arrays. We investigate in detail the electrochemical anodization of titanium in different electrolytes and its potential and temperature dependence. It turns out that due to the semiconducting properties of titania, a mirror image of the behavior of the electrically insulating porous alumina seems to be impossible. So-called porous titania in literature corresponds to the pitting regime of aluminum where pores are created due to dielectric breakdown of titania or alumina, respectively. Below the breakdown potential of titania, only thick barrier layers can be obtained. However, by nanoimprint of titanium and successive anodization below the breakdown potential, monodomain porous titanium oxide with a pore depth of 60 nm on a cm²-scale can be prepared. We discuss in detail the growth mechanism of porous structures of titanium and compare it with that of porous alumina.

© 2004 Elsevier Ltd. All rights reserved.

Keywords: Anodization; Nanoimprinted titanium; Alumina

1. Introduction

Al, Ti, Ta, Nb, V, Hf, W are classified as “valve metals” because their surface is immediately covered with a native oxide film of a few nanometers when these metals are exposed to oxygen containing surroundings [1,2]. Inherently, these oxides retard the rate of reaction on the metal surface. Therefore, they have been widely used as highly protective layers resisting corrosion. Recently, valve metals again gained considerable interest, because some oxides of valve metals have unique and excellent properties in optics, electronics, photochemistry and biology. For example, titanium oxide is a promising material for photoelectrocatalysis [3] and implants [4]. Titanium implants have been intensively investigated due to its superior strength and biocompatibility.

However, an interface layer, e.g., a hydroxyapatite (HA) coating or porous layer, on the surface of the Ti substrate is necessary to osseointegrate with bones [5] because native TiO₂ coatings have no ability to form a strong bond with bony tissue due to their low surface energy.

Current state-of-the-art techniques for aluminum anodization using self-assembly of pores allow the fabrication of monodomain and monodisperse porous alumina structures with adjustable aspect ratios [6–8]. However, porous templates based on other valve metals have been rarely studied since the 1970s. There were a few attempts to compare anodic oxide growth on other valve metals with porous alumina [9–11]. Zwilling et al. [9] reported that a porous titanium oxide layer is created in a chromic acid solution in the presence of a small amount of HF, whereas only a barrier titanium oxide layer is formed in pure chromic acid contrary to porous alumina. According to their results, the TiO₂ barrier oxide thickness is time-independent whereas the thickness of the porous oxide of titania increases with anodizing time. However, they did not mention the maximum obtainable thickness of the anodic porous titanium oxide. Gong et al. claimed that the final thickness of porous TiO₂ structures formed in dilute HF solution is independent of

* Corresponding author. Tel.: +1-626-395-2207; fax: +1-626-577-8442.

E-mail address: jinsub@caltech.edu (J. Choi).

¹ Present address: Nanofabrication Group, Division of Engineering and Applied Science, California Institute of Technology, Pasadena, CA 91125, USA.

² Present address: Fuel Cell Research Center, Korea Institute of Science and Technology (KIST), Seoul 136-791, South Korea.

the anodizing time [10]. They discussed that the dissolution rate of the formed TiO_2 oxide is very high in HF even in the absence of an anodizing process. More recently, Beranek et al. have shown that highly ordered porous titania can be produced in H_2SO_4 electrolytes containing HF. However, the thickness of pores is still limited up to 500 nm [11].

The understanding of the parameters ruling self-ordering as well as nanoimprint lithography to fabricate perfectly ordered porous alumina templates are well understood to date [12,13]. Application of this understanding to other valve metals would be very helpful not only to fabricate self-ordered porous oxides grown on other valve metals, but potentially also to improve the understanding of the growth of porous alumina. In this work, porous anodic oxide layer grown on titanium by electrochemical methods will be studied and compared to the mechanism governing the formation of porous alumina.

2. Experimental

2.1. Preparation of polished substrates

High purity titanium foil (99.99%) with a thickness of 0.5 mm was purchased from Alfa Aesar Inc. After mounting the foil on a 4-in. glass substrate, it was mechanically lapped and polished using an alumina suspension with $0.04\ \mu\text{m}$ grains (OPS suspension, Struers) for 5 h. Afterwards, the mechanically polished Ti was released from the glass substrate

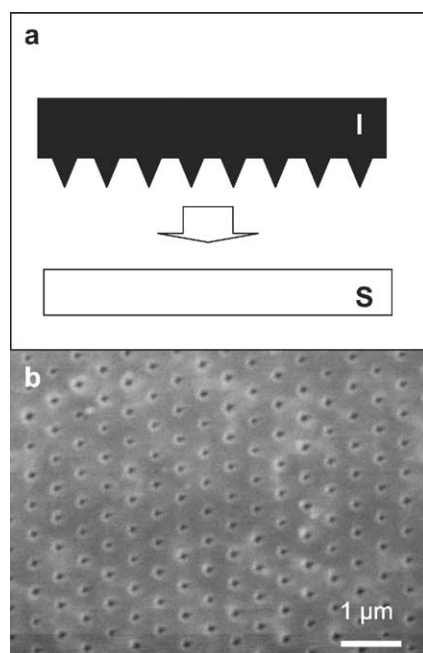


Fig. 1. (a) Schematic diagram of the indentation of Ti under a pressure of $25\ \text{kN/cm}^2$. I: imprint master stamp consisting of a hexagonal array of pyramids of Si_3N_4 with a height of 260 nm and a lattice constant of 500 nm. S: mechanically polished Ti substrate. (b) Scanning electron microscope (SEM) image of the nanoindented surface of the Ti substrate.

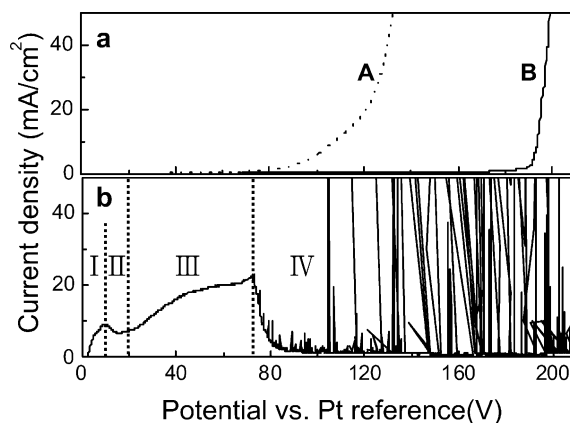


Fig. 2. Linear sweep voltammogram (LSV) of aluminum and titanium. LSV was conducted with the sweep rate of $0.1\ \text{V/s}$ in the range from 0 to 210 V: (a) LSV of aluminum (A) $0.26\ \text{M}\ \text{K}_2\text{HPO}_4$ at $60\ ^\circ\text{C}$ and (B) $0.1\ \text{M}\ \text{H}_3\text{PO}_4$ at $5\ ^\circ\text{C}$. (b) LSV of titanium at $60\ ^\circ\text{C}$ in $4\ \text{M}\ \text{H}_3\text{PO}_4$. The LSV can be divided to four regions: amorphous oxide formation (Regime I), transformation into anatase or formation of anatase in addition to the existing amorphous oxide (II–III), and transformation into rutile (IV) (Refs. [16–19]).

in a non-solvent cleaning fluid (Logitech Ltd., UK) at $80\ ^\circ\text{C}$. Then, it was cut into squares ($2\ \text{cm} \times 2\ \text{cm}$) with a mechanical cutter (Proform AG, Feather Products Modellbahnen GmbH, Switzerland). Electropolishing [14] was skipped because it would yield an inhomogeneous oxide layer on the titanium substrate.

2.2. Imprint

The fabrication procedure of a master stamp was described in detail elsewhere [7]. The master stamp consists of Si_3N_4 pyramids, which are wafer-bonded to a 4-in. silicon substrate. The pyramids have a height of 260 nm and are arranged in a hexagonal lattice with a nearest neighbor distance of 500 nm. Before indentation, dust on the surface was removed by a strong stream of N_2 gas. Subsequently,

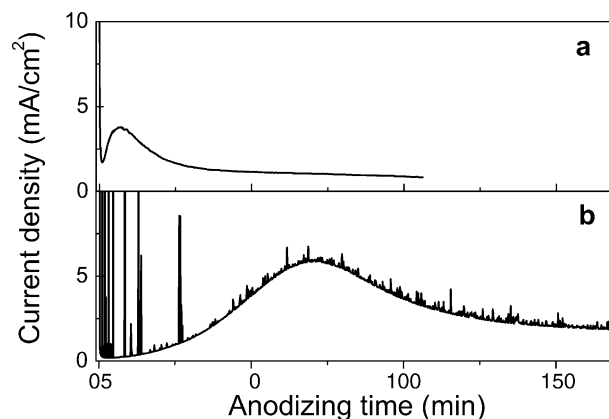


Fig. 3. Current density transients as a function of anodizing time in $4\ \text{M}\ \text{H}_3\text{PO}_4$ at 40 V (a) and at 210 V (b), which correspond to Regime III and Regime IV, respectively.

a piece of the stamp ($1\text{ cm} \times 1\text{ cm}$) was placed on the mechanical polished Ti. The pattern on a master stamp was transferred onto the surface of the titanium foil by applying a pressure of 25 kN/cm^2 using an oil press (PW, Paul-Otto Weber GmbH, Germany) as shown in Fig. 1. The average depth of the pits is around 50 nm.

2.3. Anodization and analysis

The Ti substrate was anodized under a constant cell voltage in aqueous phosphoric acid (1–4 M H_3PO_4) or ethanolic hydrofluoric acid (0.5 M HF), using a potentiostat (Keithley 2400) interfaced to a computer. The cell is a two-electrode system consisting of a Pt mesh acting as the counter electrode and Ti as the working electrode. During the anodization, the temperature and velocity of stirring of the electrolyte were kept constant. The morphologies of the porous titanium oxide were characterized by a scanning electron microscope (SEM, JEOL JSM-6300F). The thickness and composition of titanium oxide formed at different potentials were measured by Auger electron spectroscopy (Physical Electronics, PHI 600). The depths of the pores formed in ethanolic HF were analyzed by atomic force microscopy (AFM, Digital Instruments 5000 microscope)

stat (Keithley 2400) interfaced to a computer. The cell is a two-electrode system consisting of a Pt mesh acting as the counter electrode and Ti as the working electrode. During the anodization, the temperature and velocity of stirring of the electrolyte were kept constant. The morphologies of the porous titanium oxide were characterized by a scanning electron microscope (SEM, JEOL JSM-6300F). The thickness and composition of titanium oxide formed at different potentials were measured by Auger electron spectroscopy (Physical Electronics, PHI 600). The depths of the pores formed in ethanolic HF were analyzed by atomic force microscopy (AFM, Digital Instruments 5000 microscope)

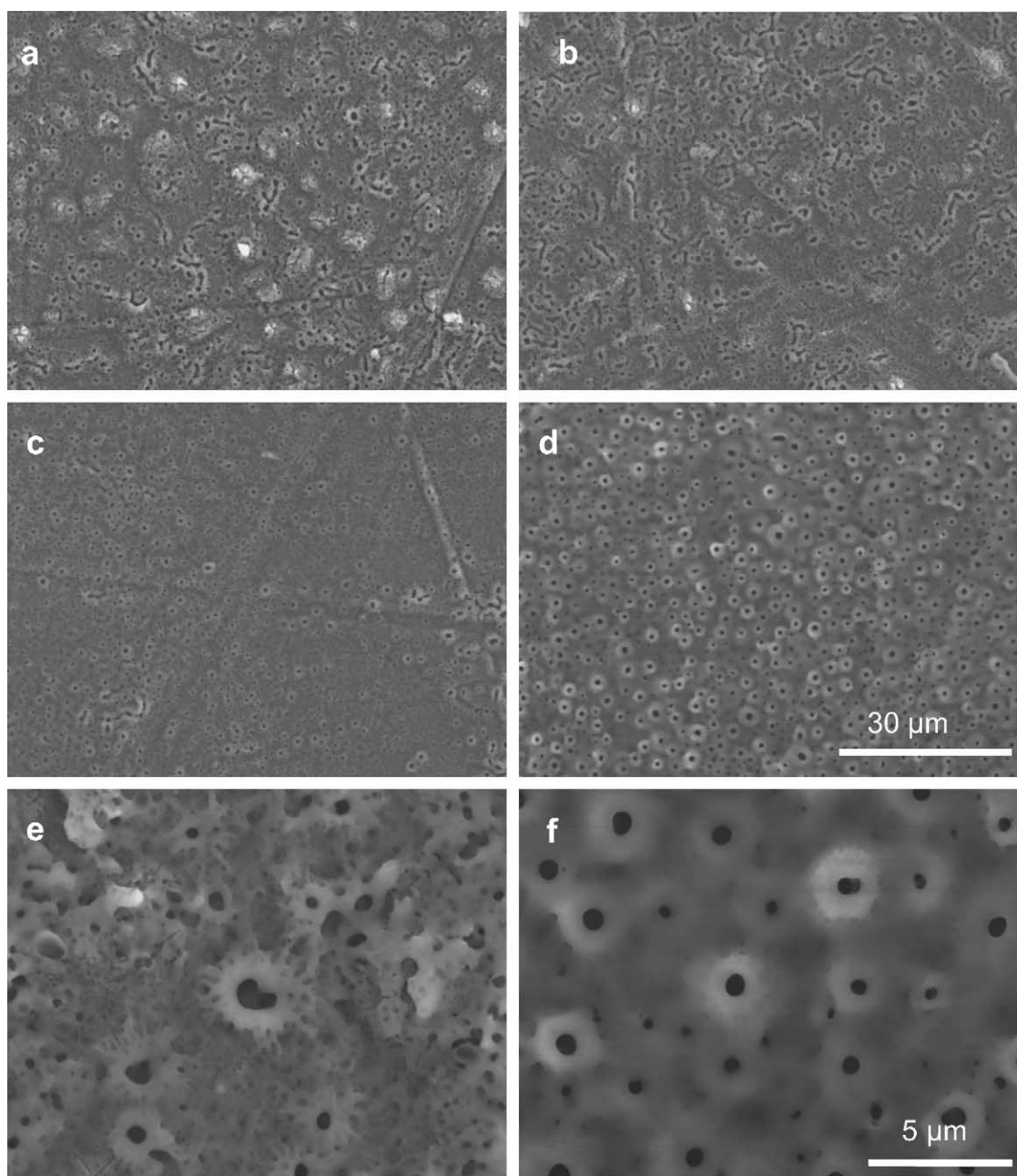





Fig. 4. Scanning electron microscope (SEM) images of titanium anodized in 1 M phosphoric acid at 210 V for 120 min: (a) 5 °C, (b) 20 °C, (c) 45 °C, (d) 60 °C, (e) and (f) are enlarged view of (a) and (d), respectively. The scales in (a–d) are identical. The scale of (e) is the same with that of (f).

Table 1
Regimes of the anodic treatment of aluminium (Ref. [28])

| | Compact alumina structures (so called barrier alumina oxides) | Thick porous alumina structures with barrier layers | Aluminum etch tunnel or aluminum dissolution |
|----------------------|---|---|---|
| Schematic pictures |  |  |  |
| Type of electrolytes | Very weak acidic or neutral solutions | Medium or weakly acidic solutions | Strong acidic solutions containing Cl ⁻ |
| Pore density | No pores | Constant with increasing anodizing time | Increase with increasing anodizing time |
| Thickness | Determined by applied potential | Determined by anodization time | Determined by diffusion limits of electrolytes |
| | | | Breakdown potential |

using standard Si₃N₄ tips. The scanning speed of AFM was 0.5 Hz.

3. Results and discussion

3.1. Pore formation above the breakdown potential of the anodic oxide

3.1.1. Influence of the potential

Titanium anodization is influenced by the growth mode, for example, constant potential, constant current density or a combination of these methods [15]. Here, we only focus on the constant potential method to compare the fabrication process with that of porous alumina.

To investigate the effect of the cell voltage, linear sweep voltammetry (LSV) with the sweep rate of 0.1 V/s was performed in the range of 0 V to 210 V in 4 M phosphoric acid at a constant temperature of 60 °C. To avoid the influence of a reaction at the counter electrode on the LSV, a Pt wire acting as a quasi-reference electrode was inserted to the two-electrode cell, placed adjacent to the working electrode. The sweep ramp has directly been superimposed on the cell voltage.

LSV of aluminum in 0.1 M H₃PO₄ and 0.26 M K₂HPO₄ shows the typical behavior of anodic oxides (Fig. 2a). Initially, the current is very low and then suddenly increases close to the breakdown potential of the anodic oxide. In the case of titanium (Fig. 2b) four different regimes can be observed, indicating that there are transitions in the structure

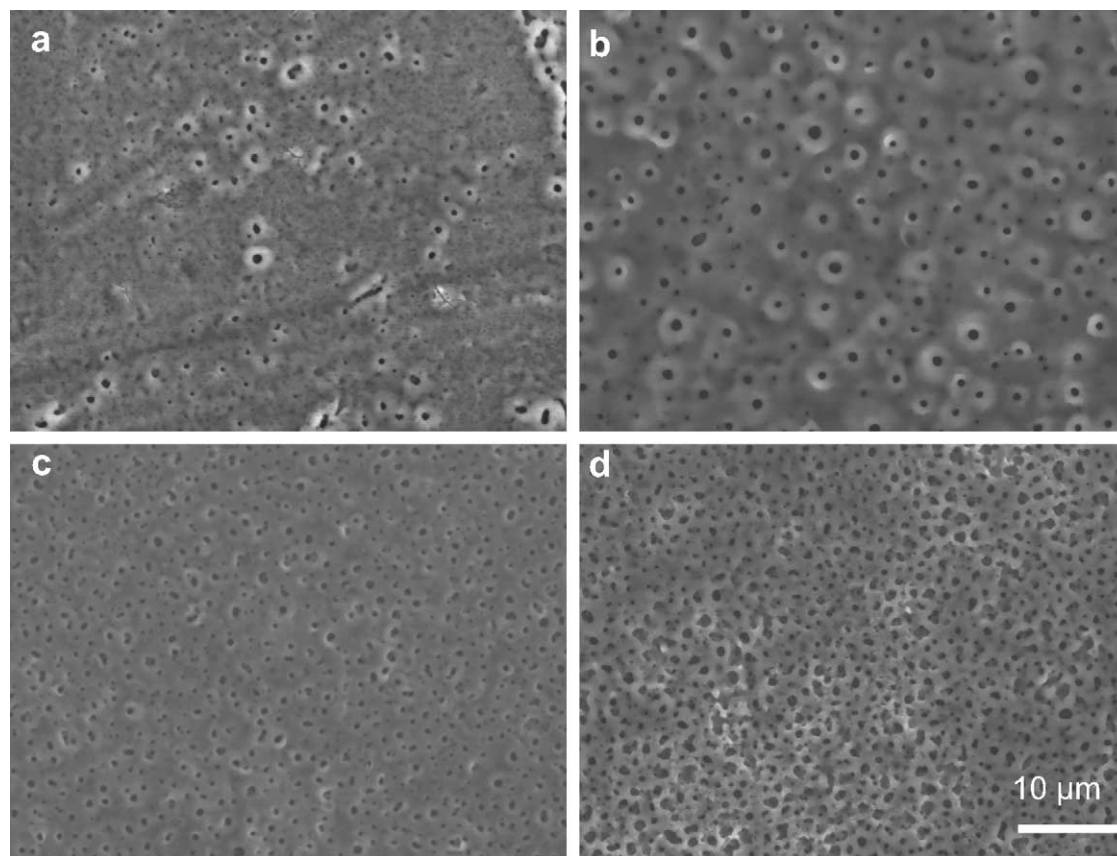


Fig. 5. SEM top views of titanium anodized for different times. Anodization (210 V, 60 °C, 1 M phosphoric acid) was performed for: (a) 45 min (b) 120 min and (c) 1000 min (d) 3500 min.

or new crystalline phases are formed in addition to the already existing amorphous layer during the anodization. In addition, it is observed that the current density below the breakdown potential is much higher than in the case of aluminum. This demonstrates the higher conductivity of titanium oxide with respect to alumina. It has been reported that in the case of the anodization of titanium, the oxide exhibits a phase transition with increasing potential from an amorphous phase into a crystalline phase such as anatase or rutile [16–18] (brookite structure was rarely mentioned). Moreover, it has been reported that the electronic resistivity of the rutile phase is three order of magnitude higher than that of anatase (at 100 °C) [19]. We assume that the ionic resistivity of the rutile phase is higher than that of anatase since rutile TiO_2 (4.25 g/cm^3) is a denser and thermodynamically more stable phase than anatase TiO_2 (3.9 g/cm^3) [19]. The decrease in the current density in the regime IV of Fig. 2b can be attributed to the transition of the anatase (or anatase + amorphous) phase into the rutile phase. The exact potentials of the phase change depend on the anodization conditions such as electrolyte and temperature [20,21]. There are few research works on the anodization of titanium in phosphoric acid [22]. However, several results obtained in other electrolyte systems might be taken into account. For example, Arsov et al. reported that during the anodization of titanium in sulfuric acid, amorphous oxides are formed below 20 V, mixed oxide between 20 and 50 V and fully crystalline anatase at voltages higher than 50 V. In the graph of Fig. 2b, a sparking of the current is observed at potentials higher than 80 V, indicating that the breakdown potential might be around 80 V. Interestingly, porous titania structures are only obtained at potentials where sparking is observable. This is in agreement with the observation that pore-like morphologies in titanium are only formed above 100 V (sparking potential region) in sulfuric acid [23]. The breakdown potential observed during titanium of the anodization has been proposed to be related to the crystallization which leads to compressive stress in the oxide or oxygen evolution [17,24,25].

Fig. 3a and b show transients of the current density as a function of anodizing time at constant cell potentials of 40 and 210 V, respectively. For 210 V anodization, sparking is observed from the beginning of anodization whereas there is no sparking in the case of 40 V.

3.1.2. Influence of the temperature

In the case of the anodization of aluminum, the temperature is typically kept below room temperature during the anodization to prevent the formed oxide from being dissolved in an acidic solution. For example, if a porous alumina structure is formed at 65 °C in sulfuric acid, the porous alumina thickness does not increase because the rate of dissolution equals that of the growth of porous alumina [26,27]. Furthermore, a constant temperature at the pore tips maintains a homogenous field-enhanced dissolution over the entire area,

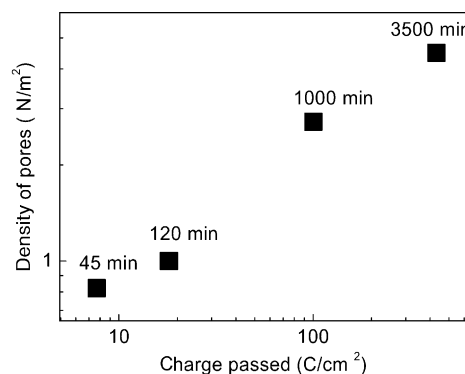


Fig. 6. Statistic analysis of the density of pores shown in Fig. 5. Note that the pore density in porous alumina formed at 195 V (ideal case) is $4.61 \times 10^{12} \text{ m}^{-2}$.

resulting in a porous alumina structure with straight pore channels and a narrow pore size distribution of the pore size.

Anodization of titanium was performed at 210 V in 1 M phosphoric acid at various temperatures. In Fig. 4, we observe that porous titania structures formed at relative low temperatures have veins of interconnected pores (or craters) and cracks caused by mechanical stress (Fig. 4a and b). In addition, thick rims around the craters with a diameter on the μm -scale are observed in the enlarged view of the SEM image (Fig. 4e). In contrast, pore like morphologies are created over the entire area at higher temperature (Fig. 4c,d and f), even though the distribution of pore sizes is relative

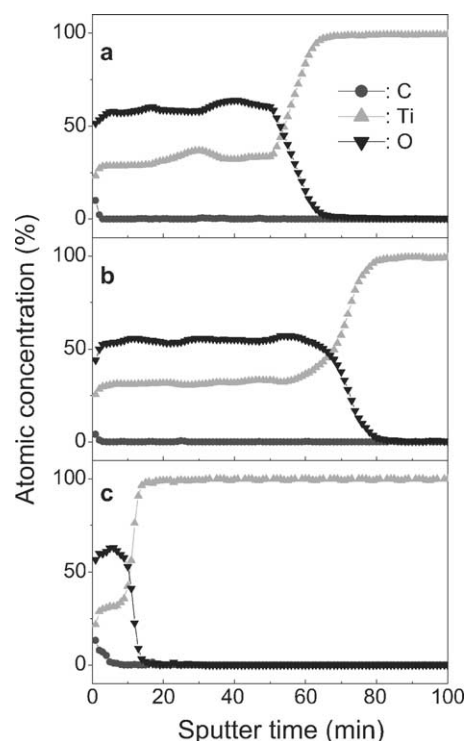


Fig. 7. Auger electron spectroscopy (AES) depth profiles for oxide layers grown on titanium under different anodization conditions: (a) 210 V, 120 min, (b) 210 V, 1000 min and (c) 80 V, 240 min.

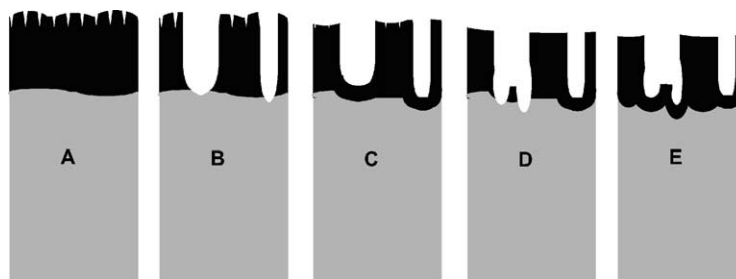


Fig. 8. Schematic diagram of porous titanium oxide formation above the breakdown potential: (A) oxide growth to maximal thickness, (B) burst of oxide by the formation of crystallites (pore formation), (C) immediate repassivation of pore tips, (D) burst of repassivated oxide, and (E) dissolution of the formed oxide and second repassivation.

broad. If the temperature is too high ($T > 70^\circ\text{C}$), the rate of the dissolution would be as fast as that of the oxide growth.

3.1.3. Comparison with alumina anodization

Since titanium oxide is a n-type semiconductor (with a high donor density in the range of 2 to $6 \times 10^{20} \text{ cm}^{-3}$, bandgap: 3.2–3.8 eV) [15], the electronic current is expected to be significantly larger than in the case of aluminum anodization (bandgap: 7–9.5 eV). Note that for insulating metal oxides, since the electronic conductivity is very low, the ionic current density predominantly transports the charges. Secondly, different phases are observed in anodic titanium oxides formed in phosphoric acid, depending on the applied potential or current density, whereas in the case of anodic aluminum the amorphous phase can mostly be obtained in phosphoric acid.

It is well known that electrochemical anodic treatments of aluminum can be classified into three categories with respect to the formation of pits, pores, or a barrier layer (Table 1) [28]: (1) compact alumina structures (so called barrier oxides) in very weak acidic or neutral solutions such as H_3BO_3 or ammonium tartrate; (2) thick porous alumina structures with barrier layers at the interface Al/electrolyte in medium or weakly acidic solutions (slightly soluble in these electrolytes) such as H_2SO_4 , $(\text{COOH})_2$, or H_3PO_4 ; (3) aluminum etch tunnels (pits) or aluminum dissolution by wet-etching in strong acidic or basic solutions such as HCl or NaOH [29].

Note that porous titanium oxide structures are created above the breakdown potential, whereas porous aluminum oxide is ordered below the breakdown potential. Aluminum dissolution occurs above the breakdown potential. The breakdown potential of Al_2O_3 strongly depends on the electrolyte and temperature, and is, for example, more than 500 V in non-dissolving electrolytes like H_3BO_3 but only a few mV in HCl [27,28].

These different growth regimes also influence the pore density. In the case of porous alumina growth occurring below the breakdown potential, pores grow continuously with time (category 2 of Table 1). The formation of new pores on the surface can be neglected. The formed oxide layer acts as an insulator to the flow of an ionic current. Thus, the reactions only occur at the pore bottom where a relatively thin

oxide exists. However, in the case of aluminum dissolution above the breakdown potential, tunnel growth competes with the formation of new pits since unetched areas between tunnel pits are not insulating (category 3 of Table 1). Therefore, the density of pits on the surface increases with Al etching time [30].

In the case of titanium anodization, the density of pores formed above the breakdown potential increases with time, which is similar to the formation of etch tunnels in Al (Fig. 5). In Fig. 6, the density of pores in titania is analyzed as a function of the quantity of charge passed during anodization. The logarithm of pore density increases linearly as a function of the logarithm of the charge. In addition, it is observed that new pores inside existing pores are created.

The thickness of the grown oxide on titanium has a maximum thickness which is mainly determined by the applied potential (2.5–3 nm/V) [2,20,31] but not by the anodizing time. In the case of alumina growth, the thickness of porous alumina increases with anodizing time but that of the barrier oxide is solely determined by the applied potential [27,28]. Fig. 7 shows Auger depth profiles, demonstrating that the thickness of the anodic oxide on titanium depends on the applied potential rather than on the anodizing time. Assuming that all the samples formed at 210 V for 120 min or 1000 min and at 80 V for 240 min consist of the rutile phase, we expect the rate of sputtering during the Auger depth profile to be the same. We observe that there is hardly any difference in the oxide thicknesses with increasing anodization time for a fixed potential (Fig. 7a and b). Fig. 7c shows that a much thinner oxide will be produced when the anodization is carried out at a lower potential even though the anodization time is twice as long as for the sample in Fig. 7a.

3.1.4. Growth models

The electrochemistry of growth of porous titanium oxide at high potentials is quite different to that of porous aluminum oxide because porous titanium oxide is formed above the breakdown potential. The development of a porous titania layer on the surface of titanium might be described as follows. Initially, the thickness of a non-porous, barrier titania grows larger with increasing anodizing voltage. Then, its structure undergoes transitions (Fig. 8A). When it is

transformed to a dense crystalline structure such as anatase or rutile, the compressive stress in the oxide increases significantly. Breakdown of the barrier oxide film occurs and new pores in between crystallites are formed (Fig. 8B). This corresponds to the occurrence of the sparking. However, the areas of electrical breakdown of the oxide are immediately covered with titanium oxide again (repassivation, Fig. 8C) due to the characteristics of valve metals. When the breakdown occurs again inside the repassivated pores (Fig. 8D and E), it looks like there is the formation of small pores inside the pores. Since current can flow through the whole oxide layer, the thickness of oxide can not linearly increase with anodizing time.

3.2. Pore formation below the breakdown potential of the anodic oxide

Since pores are randomly formed above the breakdown potential as discussed in the previous section, the anodization of lithographically structured titanium can not lead to titania templates with an arrangement of pores. In this section, the anodization of nanoindented titanium below the breakdown

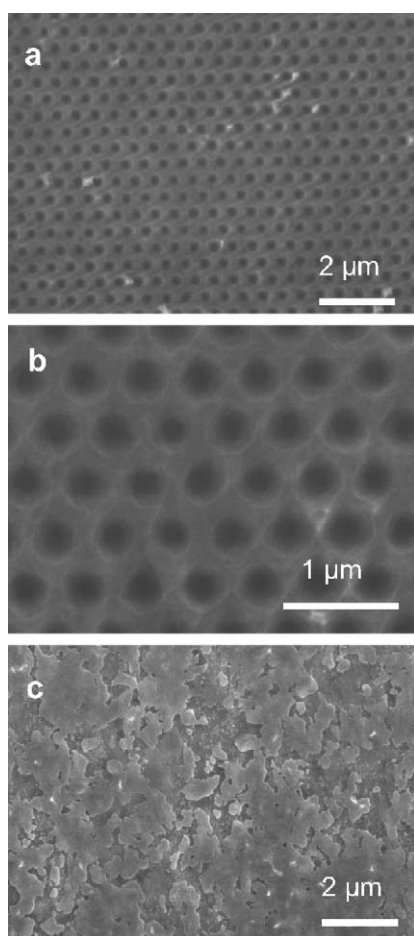


Fig. 9. SEM images of anodization of the titanium at 10 V having a lattice constant of 500 nm: (a) in ethanolic 0.5 M HF for 240 min, (b) enlarged view of (a) and (c) in aqueous 0.5 M HF for 20 min.

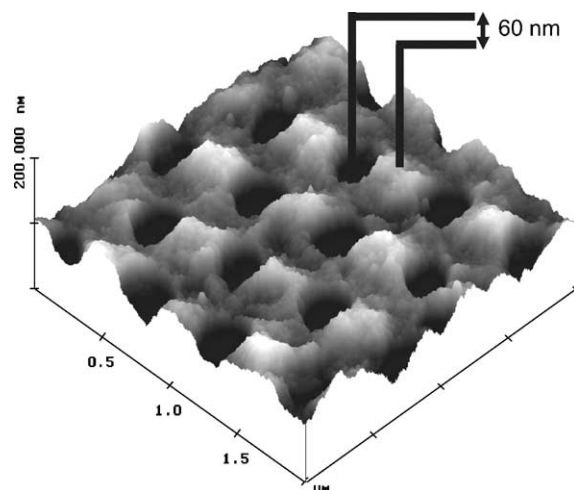


Fig. 10. Atomic force microscopy (AFM) topography of a titanium oxide array with 500 nm periodic pores. The average depth of pores is about 60 nm.

potential is studied to fabricate porous titania templates with monodomain pore arrangement.

In Fig. 9a, a titanium oxide array with 500 nm interpore distance is shown which has been anodized in ethanolic 0.5 M HF at room temperature for 240 min at 10 V. Ethanol based electrolytes were used since anodization in aqueous HF electrolyte below the breakdown potential yields a coarse oxide layer on the surface of titanium (Fig. 9c). Under these conditions, the prepatterns on the Ti substrate disappear and porous structures like those formed above the breakdown potential are not created. This originates from the very fast dissolution rate of titanium oxide in aqueous HF. In the case of anodization in ethanolic HF, an oxide layer is formed which maintains the structure of the prepattern. AFM analysis reveals an average depth of the pores of about 60 nm after 240 min anodization (Fig. 10). The oxide formation on the surface can be confirmed by AES analysis (Fig. 11). Even though the deviation of the initial size of prepatterned holes is large at the beginning of anodization, the sizes become identical during the anodization. However,

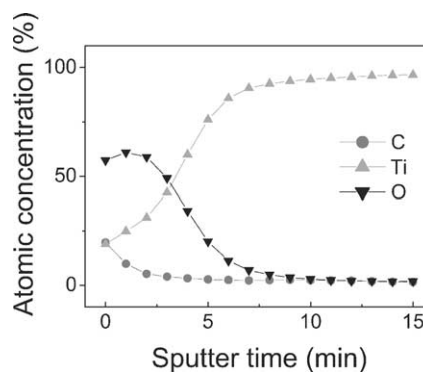


Fig. 11. Auger electron spectroscopy (AES) depth profiles for oxide layers grown on titanium in ethanolic 0.5 M HF at 10 V for 240 min.

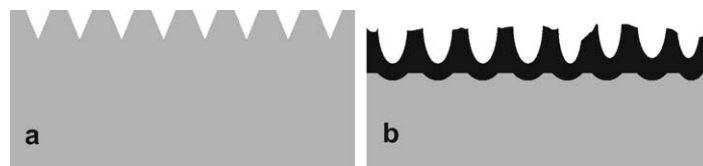


Fig. 12. Schematic diagram of the formation of barrier titanium oxide below the breakdown potential: (a) imprinted Ti substrate before anodization, and (b) oxide growth in inverted prepatterns after anodization.

after a long time anodization (>5 h), the monodomain titania structure becomes flat and eventually disappears due to the dissolution of the titanium oxide film. Note that the rectangular shape of the original prepatterns on the surface of the Ti substrate is changed into a more circular-like shape during the anodization (Fig. 9b). This is also observed during the anodization of prepatterned aluminum [7]. Note that the areas which are not imprinted by the stamp have no pores and stay flat even after anodization, demonstrating the formation of barrier oxide under these conditions (Fig. 12).

4. Conclusions

We have investigated in detail the electrochemical anodization of titanium in different electrolytes, and their potential and temperature dependence. It turned out that due to the semiconducting properties of titania, a mirror image of the behavior of porous alumina cannot be accomplished. So-called porous titania in literature corresponds to the pitting regime of aluminum where pores are created due to dielectric breakdown of titania or alumina, respectively. Below the breakdown potential of titania, only thick barrier layers can be formed. However, by nanoimprint of titanium and successive anodization of titania below the breakdown potential, monodomain porous titanium oxide with a pore depth of 60 nm on a cm^2 -scale can be prepared. We believe that this work is a first milestone on the way to find new ordered porous structures for different valve metals.

Acknowledgements

Authors thank Mr. A. Sobbe for the mechanical polishing of Ti, Dr. M. Reiche for fabricating the imprint master stamp and G. Sauer of the University Erlangen-Nuremberg for stimulating discussions.

References

- [1] J.W. Schultz, M.M. Lohrengel, *Electrochim. Acta* 45 (2000) 2499.
- [2] A. Aladjem, *J. Mater. Sci.* 8 (1973) 688.
- [3] R. Asahi, T. Morikawa, T. Ohwaki, K. Aoki, Y. Taga, *Science* 293 (2001) 269.
- [4] T. Albrektsson, P.I. Branemark, H.A. Hansson, J. Lindstrom, *Acta Orthop. Scand.* 52 (1981) 155.
- [5] H.M. Kim, F. Miyaji, T. Kokubo, T. Nakamura, *J. Biomed. Mater. Res.* 32 (1996) 409.
- [6] H. Masuda, H. Yamada, M. Satoh, H. Asoh, M. Nakao, T. Tamamura, *Appl. Phys. Lett.* 71 (1997) 2770.
- [7] J. Choi, K. Nielsch, M. Reiche, R.B. Wehrspohn, U. Gösele, *J. Vac. Sci. Technol. B* 21 (2003) 763.
- [8] J. Choi, G. Sauer, K. Nielsch, R.B. Wehrspohn, U. Gösele, *Chem. Mater.* 15 (2003) 776.
- [9] V. Zwilling, E. Darque-Ceretti, A. Boutry-Forveille, D. David, M.Y. Perrin, M. Aucouturier, *Surf. Interface Anal.* 27 (1999) 629.
- [10] D. Gong, C.A. Grimes, O.K. Varghese, W.C. Hu, R.S. Singh, Z. Chen, E.C. Dickey, *J. Mater. Res.* 16 (2001) 3331.
- [11] R. Beranek, H. Hildebrand, P. Schmuki, *Electrochim. Solid-State Lett.* 6 (2003) B12.
- [12] K. Nielsch, J. Choi, K. Schwirn, R.B. Wehrspohn, U. Gösele, *Nano Lett.* 2 (2002) 677.
- [13] O. Jessensky, F. Müller, U. Gösele, *J. Electrochem. Soc.* 145 (1998) 3735.
- [14] A.P. Li, F. Müller, A. Birner, K. Nielsch, U. Gösele, *J. Appl. Phys.* 84 (1998) 6023.
- [15] J.-L. Delplancke, A. Garnier, Y. Massiani, R. Winand, *Electrochim. Acta* 39 (1994) 1281.
- [16] T. Shibata, Y.C. Zhu, *Corros. Sci.* 37 (1995) 133.
- [17] J.-L. Delplancke, R. Winand, *Electrochim. Acta* 33 (1988) 1539.
- [18] C.E.B. Marino, E.M. de Oliveira, R.C. Rocha-Filho, S.R. Biaggio, *Corros. Sci.* 43 (2001) 1465.
- [19] H. Tang, K. Prasad, R. Sanjinbs, P.E. Schmid, F. Lévy, *J. Appl. Phys.* 75 (1994) 2042.
- [20] L. Arsov, M. Froelicher, M. Froment, A.H.-L. Goff, *J. de Chim. Phys.* 72 (1975) 275.
- [21] G. Blondeau, M. Froelicher, M. Froment, A.H.-L. Goff, *Thin Solid Films* 42 (1977) 147.
- [22] Y.T. Sul, C.B. Johansson, Y. Jeong, T. Albrektsson, *Med. Eng. Phys.* 23 (2001) 329.
- [23] J.C. Marchenoir, J.P. Loup, J. Masson, *Thin Solid Films* 66 (1980) 357.
- [24] J. Yahalom, J. Zahavi, *Electrochim. Acta* 15 (1970) 1429.
- [25] J.F. MaAleer, L.M. Peter, *J. Electrochem. Soc.* 129 (1982) 1252.
- [26] J. Choi, K.H. Lee, Y. Tak, *Electrochemistry* 69 (2001) 843.
- [27] J.W. Diggle, T.C. Downie, C.W. Couling, *Chem. Rev.* 69 (1969) 365.
- [28] P.A. Malachuk, in: A.J. Bard (Ed.), *Encyclopedia of Electrochemistry of the Elements*, vol. VI, Marcel Dekker, New York, 1973, p. 63.
- [29] R.B. Wehrspohn, A.P. Li, K. Nielsch, F. Müller, W. Erfurth, U. Gösele, in: K.R. Hebert, R.S. Lillard, B.R. Mac Dougall (Eds.), *The Electrochemical Society Proceeding Series, PV 2000-4*, Pennington, NJ, 2000, p. 271.
- [30] R.S. Alwitt, H. Uchi, T.R. Beck, R.C. Alkire, *J. Electrochem. Soc.* 131 (1984) 13.
- [31] M. Kozłowski, W.H. Smyrl, L.J. Atanasoka, R. Atanasoki, *Electrochim. Acta* 34 (1989) 1763.